Modeling topographical density for geoid determination

Robert Kingdon[1], *Petr Vaníček*[2], *Marcelo Santos*[3]

Robert Kingdon[1], Petr Vaníček and Marcelo. Department of Geodesy and Geomatics Engineering, University of New Brunswick, Fredericton, NB E3B 5A3, Canada

[1]Corresponding author (e-mail: robert.kingdon@unb.ca)

Modeling topographical density for geoid determination

Robert Kingdon, Petr Vaníček and Marcelo Santos

Abstract: In geoid computation, effects of real 3-dimensional topographic masses on the Earth's gravity field must be accurately quantified and, in the Stokes-Helmert scheme, replaced with effects of those masses condensed on the geoid. The most comprehensive modern schemes for evaluation of topographical effects account for terrain effects, use a spherical model of topography, and incorporate 2-dimensionally varying models of topographical mass-density. In this contribution, we employ a 3-dimensionally varying model of topographical density. We use Newton's integration to determine the Direct Topographical Effect (DTE) on gravity and Primary Indirect Topographical Effect (PITE) on gravity potential. Finally, we apply Stokes' integration to calculate the DTE, PITE and Secondary Indirect Topographical Effect (SITE) on geoidal height.

We focus here on validation of our results and demonstration of our software's capabilities. We present results for the simple geometrical shape of a disc under various rotations, and for the anomalous density of lake waters. Effects on geoidal height for these simulations reach centimeter level, up to 2.2 cm in magnitude. For a simulation of the effects of neglected mass anomalies of the lakes, we find results reaching 0.8 cm in magnitude. We examine the behavior of our results as calculated using various step sizes for numerical integration, and by comparing numerical results to analytical results for the specific case of a disc. These suggest that the maximum percent error of our results is about 23.5 % for the DTE on gravity, and 7.6 % for the PITE on gravity potential.

Introduction

The geoid, an equipotential surface approximating mean sea level, is a common reference surface for height systems. It is given by its vertical separation from a reference geocentric biaxial ellipsoid, that best fits to the figure of the Earth, such as the GRS-80 ellipsoid (Moritz, 1984). This separation can be determined by gravimetric, geometric or other means; here we will discuss one specific gravimetric approach: the Stokes-Helmert technique (e.g., Vaníček and Martinec 1994). This method applies the theorem of Stokes (1849) for estimation of the geoid based on gravity observations at the geoid level, but assumes no masses are present above the geoid, where gravity observations are made. To achieve this condition, the Stokes technique is applied after replacing the topographical masses (between the geoid and the Earth's surface) by an infinitesimally thin layer of horizontally varying density at or below the geoid surface. This method was originally proposed by Helmert (1884). In the Stokes-Helmert technique this condensation layer is located at the geoid surface, in what is known as Helmert's second condensation method. The effect of this change in mass distribution on gravity is called a Direct Topographical Effect (DTE). Note that there is also a corresponding Direct Atmospheric Effect (DAE), which we will not deal with here. Application of the Stokes technique to gravity anomalies that reflect this new mass distribution produces a surface that is very close to the geoid and is called co-geoid. A corrective term must be applied to the co-geoid to get the final geoid. The corrective term is called the Primary Indirect Topographical Effect (PITE).

Any topographical effect can be calculated by finding the difference between the effect of condensed masses, and the effect of real masses. Determination of the topographical effects

thus requires an accurate knowledge of the mass-density distribution within topography. The most comprehensive current evaluations of topographical effects on the geoidal height account for terrain effects, use a spherical (rather than planar) approximation of topography for determining distances, and incorporate 2-dimensionally (laterally) varying models of topographical mass-density (e.g., Vaníček et al. 1999). A laterally varying mass-density model is often used to approximate the Earth's real 3-dimensional density anomalies because it is difficult and expensive to determine the distribution of density within topography in a given area, and even where information about the distribution is known, it is not precise (Martinec 1993; Kuhn 2003).

For this investigation we are interested only in the density structure of topographical masses, since effects of any masses deeper than the geoid are already accounted for the Stokes-Helmert geoid solution. We are thus interested in knowledge of the density distribution in at most the upper 10 km of the Earth's crust, and normally at depths less than 1 km. Investigations into the structure of the Earth's crust have been ongoing over the past century using various methods (Mooney 2007). Of these methods, seismic reflection is the most relevant active seismic method of locating density interfaces in the upper crust, including the topography. Currently, seismic reflection provides horizontal and vertical accuracies of as good as 50m, though interfaces determined to this precision are not available globally (Mooney 2007). Seismic wide-angle reflection and refraction are less precise, usually applying forward modeling (e.g., Zelt 1999) and occasionally inverse methods (e.g., Zelt and Smith 1992) to determine crustal structures. Among passive seismic methods, local seismic tomography allows construction of a 3-D image of the upper crust (e.g., Salah and Zhao 2003), with horizontal resolutions of up to 25 km, and vertical resolutions of several kilometers. Seismic methods are especially valuable in conjunction with deep (3 to 12 km)

borehole sampling, which provides in situ measurements of seismic velocity and density and can act as a control for density or seismic modeling (e.g., Smithson et al. 2000). Gravity studies (e.g., Tiberi et al. 2003) complement seismic investigations for determination of crustal density structures, although it does not provide sufficient accuracy for our methods. Geological mapping is a further useful source of information on the near surface crustal density structure (Mooney 2007).

There have been some applications of these techniques to constructing regional and global crustal geology models, usually with a focus on the whole crust and even the upper mantle (e.g., Pasyanos et al. 2004, Mooney et al. 1998, Bassin et al. 2000). These consist of a series of geological boundaries between layers having different geological characteristics, but are usually directed at an understanding of the whole crust and below. The earliest global model was the 3SMAC model by Soller et al. (1982) that provided 2º x 2º cells giving density and seismic information. More recently, the CRUST 2.0 global model has been produced (Bassin et al. 2000), which represents crustal structure according to a series of 7 layers with thicknesses given in a 2º x 2º grid. Although this model is not specifically a model of topographical density, it may be useful for calculation of topographical density effects since it includes layers describing sediment thickness, and sediment represents one of the key density anomalies within topography. Kuhn (2003) has outlined a method for determining a 3-D density model specifically for geodetic purposes by interpretation of results of seismic surveys, borehole data, and geological maps, but such a model has not yet been implemented. Instead, for geodetic calculations, a laterally varying model based on surface topographical densities derived from geology maps is normally used (e.g., Huang et al. 2001).

We set aside for the time being the problem of determining exactly the real topographical mass-density distribution, and instead try to estimate the potential loss in

accuracy of geoidal heights by using a 2-dimensionally varying, rather than 3-dimensionally varying, model of topographical density (hereafter called a 2-D model and a 3-D model). By this investigation we hope to determine whether evaluation effects of 3-D density models is worthwhile. We do this by creating hypothetical but realistic density distributions, and calculating their effects on geoidal height. In these calculations, we follow roughly the approach of Martinec (1998), with some generalization where necessary, to determine effects of the topographical density accounted for in a 3-D model but unaccounted for in a 2-D model. In terms of the Stokes-Helmert scheme, we evaluate the contribution of anomalous density unaccounted for in 2-D models on the direct topographical effect (DTE) on gravity, and the primary indirect topographical effect (PITE) on gravity potential. From these, the corresponding DTE, PITE and secondary indirect topographical effect (SITE) on geoidal height can be determined by applying Stokes integration to the individual effects (e.g., Heiskanen and Moritz 1967; Vaníček and Kleusberg 1987).

In this contribution, we focus on mainly validating our application of the Newton integral for calculating effects of 3-D anomalous density on gravity and gravity potential. We limit ourselves to two families of simulations: density distributions defined by simple geometrical figures, and those defined by a single density contrast. We will primarily discuss results for the former application, only demonstrating our capacity to generate results with the latter, as we are attempting as a first step to understand the behaviour and potential order of magnitude of neglected 3-D density effects on a simple level before turning to more complex distributions. Also, applying distributions based on simple shapes allows us to easily compare some results with an analytical determination in spherical coordinates. Once our software has effectively met this first benchmark, we can rely more heavily on its results for more complex distributions.

This paper will first describe the key points of our methodology. We begin by describing the key mathematical aspects of our approach, to indicate its relation to and distinction from other density effect calculations. We conclude our discussion of methodology by describing how the technique has been implemented in our numerical calculation software, *Rad_Eff_Geoid.c*. Thereafter we present some preliminary results to demonstrate the capability of the software, followed by results of our validation attempts.

Methodology

Modeling of topographical density

Our 3-D model of topographical density represents density variation within topography by a series of surfaces, each representing a particular density contrast. For example, if we wish to model the topographical density of a region including a lake, our model consists of a horizontal surface at a height of zero (corresponding to the geoid), a surface given by the height of the lakebed, and a surface given by the height of the topography (or the lake surface, over the lake). The densities of the volumes between the layers are then specified. In the case of a lake, the density in the region above the geoid surface but below the topographical and lakebed surfaces might be assigned the commonly assumed average crustal density $\bar{\rho}$ of 2670 kg/m^3. The density in the region above the lakebed and geoid surfaces, but below the topographical surface, i.e. the lake waters, would have a density of about 1000 kg/m^3. The anomalous density in the latter region, then, would be -1670 kg/m^3.

More intricate arrangements of surfaces are also possible, though distributions based on multiple input surfaces have not been implemented in the current version of our software. We have implemented density distributions defined by simple geometrical figures. For example, we may define a disc as a body of anomalous density bounded by a cylinder and two planes. We assign the disc a large anomalous density, e.g., 660 kg/m^3, typical of a density contrast between basalt and sandstone (Parasnis 1997). Density distributions thus defined will provide the region over which our Newton integration is carried out.

The Newton kernel and its radial derivative for calculation of effects on gravity and gravity potential

The following derivations are performed in a spherical coordinate system, considered to have its origin at the geocentre, and illustrated in Fig. 1 below, with **C** indicating the coordinate system origin. We will use the coordinates $<r,\Omega = (\varphi,\lambda)>$ to represent the geocentric radius, latitude and longitude of a point of interest ***P***, also called the computation point. The coordinates $<r',\Omega' = (\varphi',\lambda')>$ will represent the coordinates of the running point in integration, ***P'***. The term $\psi(\Omega,\Omega')$ represents the spherical solid angle between these two points, given by:

[1] $$\cos\psi(\Omega,\Omega') = \cos\varphi\cos\varphi' + \sin\varphi\sin\varphi'\cos(\lambda - \lambda').$$

We will normally refer to it simply as ψ for the sake of conciseness.

We also introduce $L(r',r,\psi)$, the straight line (Euclidian) distance between the point of interest and the integration point:

$$[2] \qquad L(r',r,\psi) = \sqrt{r'^2 + r^2 - 2r'r\cos\psi}\,.$$

The gravitational potential $V(r,\Omega)$ resulting from a density distribution $\rho(r',\Omega')$ over a region $<r' \in [r_g(\Omega'),r_t(\Omega')] \cap \Omega' \in \Omega_0>$ is given by integration of the Newton kernel, $L^{-1}(r',r,\psi)$, over that region (e.g., Martinec 1998, Eq. 1.5):

$$[3] \qquad V(r,\Omega) = G \iint_{\Omega' \in \Omega_0} \int_{r'=r_g(\Omega')}^{r_t(\Omega')} L^{-1}(r',r,\psi)\rho(r',\Omega')r'^2 dr' d\Omega',$$

where $r_g(\Omega')$ and $r_t(\Omega')$ represent the geocentric radii of the geoid and topographical surfaces at the integration point, and $r_t(\Omega') = r_g(\Omega') + H_t(\Omega')$ where $r_g(\Omega')$ may be given by a geoid model and $H_t(\Omega')$ from a terrain model. For all applications described here, Ω_0 is defined by a spherical cap of constant radius centered on the point of interest.

The gravity, $A(r,\Omega)$, resulting from a mass distribution is then given by the integral over the radial derivative of the inverse of Eq. [2] multiplied by the density, which follows from Martinec (1998, Eq. 3.6):

$$[4] \qquad A(r,\Omega) = G \iint_{\Omega' \in \Omega_0} \int_{r'=r_g(\Omega')}^{r_t(\Omega')} \frac{\partial L^{-1}(r,r',\psi)}{\partial r} \rho(r',\Omega')r'^2 dr' d\Omega'.$$

Eqs. [1] to [4] will here be applied for a density distribution representing anomalous density as well. In that case, we replace $\rho(r',\Omega')$ with:

[5] $\delta\rho(r',\Omega') = \rho(r',\Omega') - \bar{\rho}$,

where we are dealing with anomalies relative so some prescribed constant density $\bar{\rho}$, or:

[6] $\delta\rho(r',\Omega') = \rho(r',\Omega') - \bar{\rho}(\Omega')$,

where we are dealing with anomalies relative to a laterally varying density distribution $\bar{\rho}(\Omega')$.

In the case of a Eq. [5], the reference density value $\bar{\rho}$ is defined such that the sum of anomalous densities (usually globally) is expected to be zero. In the case of Eq. [6], although ideally the sum of anomalous density values along any topographical column should equal to zero, e.g. by assigning to $\bar{\rho}(\Omega')$ the mean density value along the column, there is usually not sufficient information to meet this condition. Instead the density value of rock at the topographical surface is often assigned to the whole column. We will be considering anomalies defined according to Eq. [6] here.

Mathematical representation of 3-D density and condensed density models

For any integration point Ω', we can represent the radial distribution of density as a piecewise function. Let us take the simple example of a lake, as in section 2.1. Let the density of topography outside the lake be ρ_0, and the density of the lake water be ρ_1. We are dealing

here with three surfaces: the geoid surface, the lower bound of the region we are concerned with, defined by $r_g(\Omega')$; the surface of the topography and the surface of the lake, defined by $r_t(\Omega')$ and the lake bed, with geocentric radius $r_b(\Omega')$. In this case, for any point Ω' we write:

$$[7] \qquad \rho(r',\Omega') = \begin{cases} \rho_0, & r' \in [r_g(\Omega'), r_t(\Omega')] \cap \Omega' \notin \Omega_b \\ \rho_0, & r' \in [r_g(\Omega'), r_t(\Omega')] \cap r' \le r_b(\Omega') \cap \Omega' \in \Omega_b \\ \rho_1, & r' \in [r_g(\Omega'), r_t(\Omega')] \cap r' > r_b(\Omega') \cap \Omega' \in \Omega_b \\ 0, & \text{elsewhere} \end{cases},$$

where Ω_b represents the region covered by the lake, over which $r_b(\Omega')$ is defined. In some cases we may have more complicated parameters. For example, if we are dealing with a model defined by a rectangular prism under some rotations we have 6 planes to deal with, in addition to $r_g(\Omega')$ and $r_t(\Omega')$.

When we are dealing with anomalous densities, we must change somewhat the formulation of Eq. [7]. If the prescription in Eq. [5] is used, then instead of Eq. [7], we represent the anomalous density distribution by:

$$[8] \qquad \delta\rho(r',\Omega') = \begin{cases} \rho_0 - \overline{\rho}, & r' \in [r_g(\Omega'), r_t(\Omega')] \cap \Omega' \notin \Omega_b \\ \rho_0 - \overline{\rho}, & r' \in [r_g(\Omega'), r_t(\Omega')] \cap r' \le r_b(\Omega') \cap \Omega' \in \Omega_b \\ \rho_1 - \overline{\rho}, & r' \in [r_g(\Omega'), r_t(\Omega')] \cap r' > r_b(\Omega') \cap \Omega' \in \Omega_b \\ 0, & \text{elsewhere} \end{cases}.$$

If density differences are used, and if $\rho(\Omega')$ is the laterally varying density (as is often the practice, e.g., Huang et al. 2001 and Featherstone 2000), then it reads:

$$[9] \qquad \delta\rho(r',\Omega') = \begin{cases} \rho_0 - \rho_1, & r' \in [r_g(\Omega'), r_t(\Omega')] \cap r' \le r_b(\Omega') \le r_t(\Omega') \cap \Omega' \in \Omega_b \\ 0, & \text{elsewhere} \end{cases}.$$

Since we can determine the radial distribution of anomalous density at any integration point, we can also determine the resulting anomalous condensation density at any integration point. We do this by applying the general formula (e.g., Martinec 1998, Eq. 2.3):

$$[10] \qquad \delta\sigma(\Omega') = \frac{1}{r_g^2(\Omega')} \int_{r'=r_g(\Omega')}^{r_t(\Omega')} \delta\rho(r',\Omega') r'^2 dr',$$

Where $\delta\sigma(\Omega')$ is the condensation density at the point Ω'. Since for any Ω' the density can be written as a piecewise constant function, the integral in Eq. [10] can be written in a more general form for any series of surfaces:

$$[11] \qquad \delta\sigma(\Omega') = \frac{1}{r_g^2(\Omega')} \sum_{i=0}^{n-1} \int_{r'=r_i(\Omega')}^{r_{i+1}(\Omega')} \delta\rho_{i,i+1} r'^2 dr' = \frac{1}{r_g^2(\Omega')} \sum_{i=0}^{n-1} \delta\rho_{i,i+1} \frac{[r_{i+1}^3(\Omega') - r_i^3(\Omega')]}{3},$$

where $r_i(\Omega')$ is a radius vector of any surface contained within the topography at Ω', $\delta\rho_{i,j}$ is the anomalous density between surfaces i and j, n is the number of surfaces present in the topography including the geoid and topographical surface, $r_0(\Omega') = r_g(\Omega')$ and $r_n(\Omega') = r_t(\Omega')$. For our situation, where at most 4 surfaces are concerned, evaluating $\delta\sigma(\Omega')$ using Eq. [11] is trivial.

Calculations of 3-D anomalous density effects on geoid and gravity

Prescriptions for the evaluation of the DTE, PITE and SITE are given in a variety of sources (e.g., Martinec and Vaníček 1994a; Martinec and Vaníček 1994b; Sjöberg and Nahavandchi 1999); most notably in Martinec (1998) whom we follow closely here.

The DTE is simply the difference between the effect of the anomalous density of real topography and that of the condensed topography.

[12] $$\delta A_{\delta\rho}(\Omega) = A^{t}_{\delta\rho}(\Omega) - A^{c}_{\delta\rho}(\Omega),$$

on surface gravity, where the $\delta\rho$ subscripts indicate that here we are dealing with 3-D anomalous density effects, (distinct from the $\delta\ \bar{\rho}$ subscript conventionally used to denote effects of laterally varying anomalous density). $A_{\delta\rho}{}^{t}(\Omega)$ is the effect of real topography on gravity and can be found using Eq. [4]:

[13] $$A^{t}_{\delta\rho}(\Omega) = A_{\delta\rho}(r^{t}(\Omega),\Omega) = G \iint_{\Omega'\in\Omega_0} \int_{r'=r_g(\Omega')}^{r_t(\Omega')} \left.\frac{\partial L^{-1}(r,r',\psi)}{\partial r}\right|_{r=r^{t}(\Omega)} \delta\rho(r',\Omega') r'^{2} dr' d\Omega',$$

while the effect of the condensed layer, $A_{\delta\rho}{}^{c}(\Omega)$ is found by taking the limit of Eq. [4] as $r_t(\Omega)\to r_g(\Omega)$, which yields:

[14] $$A^{c}_{\delta\rho}(\Omega) = \lim_{r_t(\Omega')\to r_g(\Omega')} A_{\delta\rho}(r^{t}(\Omega),\Omega) = G \iint_{\Omega'\in\Omega_0} \left.\frac{\partial L^{-1}(r,r_g(\Omega'),\psi)}{\partial r}\right|_{r=r^{t}(\Omega)} \sigma(\Omega') r_g^{2}(\Omega') d\Omega'.$$

The values of $\delta A_{\delta\rho}(\Omega)$ can be determined, depending on the information available about anomalous density structures, by numerical integration, analytical integration, or some combination of these. In the context of this study, we have performed all integration numerically in the horizontal direction, but analytically in the vertical direction along a given column of topography. Having calculated $\delta A_{\delta\rho}(\Omega)$, we may determine the corresponding DTE on geoidal height through the Stokes' integration. The Stokes integration, in conjunction with Bruns' s formula, may be used to convert a field of effects on gravity into their effect on geoidal height. The formulation for Stokes integration to determine the DTE on geoidal height as a result of a topographical effect is given by (Martinec 1993, Eq. 4.5):

$$[15] \qquad \delta N_{DTE,\delta\rho}(\Omega) \approx \frac{R}{4\pi\gamma} \iint_{\Omega' \in \Omega_0} S(\psi)\delta A_{\delta\rho}(\Omega')d\Omega',$$

where R is the mean radius of the Earth and $S(\psi)$ is the Stokes kernel given by (e.g., Vaníček and Krakiwsky 1986):

$$[16] \qquad S(\psi) = 1 + \frac{1}{\sin\frac{1}{2}\psi} - 6\sin\tfrac{1}{2}\psi - 5\cos\psi - 3\cos\psi\ln(\sin\tfrac{1}{2}\psi + \sin^2\tfrac{1}{2}\psi).$$

The PITE is the difference between the effects of mass anomalies of real and condensed topography on gravity potential at the geoid:

$$[17] \qquad \delta V_{\delta\rho}(\Omega) = V^t_{\delta\rho}(\Omega) - V^c_{\delta\rho}(\Omega).$$

Here, we use Eq. [3] to evaluate the term $A_{\delta\rho}^{t}(\Omega)$:

$$[18] \qquad V_{\delta\rho}^{t}(\Omega) = V_{\delta\rho}(r_g(\Omega),\Omega) = G \iint\limits_{\Omega' \in \Omega_0} \int\limits_{r'=r_g(\Omega')}^{r_t(\Omega')} L^{-1}(r_g(\Omega), r', \psi)\delta\rho(r', \Omega') r'^2 dr' d\Omega';$$

and the limit of Eq. [17] as $r_t(\Omega) \to r_g(\Omega)$ to find $A_{\delta\rho}^{c}(\Omega)$:

$$[19] \qquad V_{\delta\rho}^{c}(\Omega) = \lim_{r_t(\Omega') \to r_g(\Omega')} V_{\delta\rho}(r^t(\Omega),\Omega) = G \iint\limits_{\Omega' \in \Omega_0} L^{-1}(r_g(\Omega), r_g(\Omega'), \psi)\sigma(\Omega') r_g^2(\Omega') d\Omega'.$$

For each point where the PITE on gravity potential is evaluated, the PITE on geoidal height may also be evaluated according to Bruns's formula (Martinec 1993, Eq. 4.6):

$$[20] \qquad \delta N_{PITE,\delta\rho}(\Omega) = \frac{\delta V_{\delta\rho}(\Omega)}{\gamma}.$$

The PITE on gravity is further given by:

$$[21] \qquad \delta A_{PITE,\delta\rho}(\Omega) = \frac{2}{R}\delta V_{\delta\rho}(\Omega).$$

By Stokes' integration of the PITE on gravity over a large area, we may determine the SITE on geoidal height (Martinec 1993, Eq. 4.7):

[22] $$\delta N_{SITE,\delta\rho}(\Omega) = \frac{1}{2\pi\gamma} \iint_{\Omega' \in \Omega_0} S(\psi)\delta V_{\delta\rho}(\Omega')d\Omega'.$$

Numerical evaluation of the DTE, PITE and SITE

Throughout our numerical evaluations, we consider that $r_g(\Omega') = r_g(\Omega) = R$, i.e., we employ a spherical approximation. This is common in similar calculations, e.g., of laterally varying anomalous density effects on geoidal height (e.g., Martinec 1993; Huang et al. 2001), and although we have not rigorously tested its validity here we consider the approximation still appropriate as we are only performing a first estimation of 3-D anomalous density effects.

Horizontal numerical integration is required for Eqs. [13], [14], [18] and [20]. All numerical integration is performed using spherical coordinates φ' and λ', with the areal element $d\Omega' = \sin\varphi' d\varphi' d\lambda'$. Testing has shown that the local density bodies we are modeling (most less than 100 km wide, and less than 1 km thick) do not have a significant effect beyond 3° from the computation point, and so integration is limited to a 3° cap. The cap is divided into four circular zones centered on the computation point: the middle zone, inner zone, innermost zone, and a zone comprising only the near vicinity of the computation point. The sizes and resolutions of these zones may be modified in the option file of our software. Through testing, we have determined suitable resolutions and sizes for each of these zones, as indicated in Table 1. These radii were determined by increasing each until the change in the results was negligible. So, for example, starting with a middle zone radius of 3600 arcseconds, we then increased it by intervals of 1800 arcseconds until the difference in results after a particular increase was negligible. We determined that the difference in results was negligible when

increasing the radius from 5400 arcsecond to 7200 arcseconds, and so we considered 7200 arcseconds a sufficient radius.

Eqs. [13] and [18], which appear to require a 3-D numerical integration, can be reduced to only 2-d integrations by taking advantage of the aforementioned behavior of $\delta\rho(r',\Omega')$ as a piecewise constant function of argument Ω'. Analogous to the development of Eq. [11] we can write, e.g., for Eq. [13]:

$$[23] \qquad \int_{r'=R}^{r_t(\Omega')} \left.\frac{\partial L^{-1}(r,r',\psi)}{\partial r}\right|_{r=r'(\Omega)} \delta\rho(r',\Omega')r'^2 dr' = \sum_{i=0}^{n-1} \delta\rho_{i,i+1} \left.\frac{\partial \tilde{L}^{-1}(r,r',\psi)}{\partial r}\right|_{r'=r_i}^{r_{i+1}} \Bigg|_{r=r'(\Omega)},$$

where, as provided by Martinec (1993, Eq. 2.22):

$$[24] \qquad \frac{\partial \tilde{L}^{-1}(r,r',\psi)}{\partial r} = \frac{(r'^2+3r^2)\cos\psi + (1-6\cos^2\psi)rr'}{L(r,r',\psi)} + r(3\cos^2\psi - 1)\ln\left|r' - r\cos\psi + L(r,r',\psi)\right|.$$

Similarly, for Eq. [17] we can write:

$$[25] \qquad \int_{r'=R}^{r_t(\Omega')} L^{-1}(R,r',\psi)\delta\rho(r',\Omega')r'^2 dr' = \sum_{i=0}^{n-1} \delta\rho_{i,i+1} \tilde{L}^{-1}(R,r',\psi)\Big|_{r'=r_i}^{r_{i+1}},$$

and according to Martinec (1993, Eq. 2.20):

$$[26] \qquad \tilde{L}^{-1}(r,r',\psi) = \frac{(r' + 3r\cos\psi)}{2} L(r,r',\psi) + \frac{r^2(3\cos^2\psi + 1)}{2} \ln\left|r' - r\cos\psi + L(r,r',\psi)\right|.$$

Thus numerical integration is only necessary to carry out horizontally.

In cases where the topographical density distribution is given by a surface or series of surfaces, the accuracy of determination of Eq. [13] and [18] could theoretically be further improved by representing the surface as a polyhedral body. The integration over a polyhedral body of constant density can be carried out analytically in all three dimensions in a Cartesian coordinate system (e.g., Paul 1974), and even over a polyhedral body of linearly varying density (Pohanka, 1998). Previous studies have shown that the polyhedral representation provides an improvement in the case of terrain effect calculations (e.g., Tsoulis, 2001), when applied in a local planar coordinate system. Unfortunately, this analytical integration over polyhedrons has not yet been developed in spherical coordinates, and since the development cannot be done over relatively simple prismoidal bodies (Heck and Seitz 2007) it may be impossible. We have not investigated the possibility of using the analytical integration in e.g., a global Cartesian coordinate system. While the existing developments could be applied for calculating effects of real topography using polyhedral models, and may be useful for validation in the future, we are aware of no formulation for corresponding effects of condensed topography. Since this is only our first attempt at modeling 3-D density effects, we have not attempted these developments. We also are unable to apply an analytical integration over each (prismoidal) cell in the three-dimensional integration of Eq. [13] and [18]. While Nagy et al. (2000) provide formulas for this approach in a rectangular coordinate system, the horizontal integration over a cell cannot be carried out analytically in a spherical coordinate system, and so numerical integration is necessary (Heck and Seitz 2007).

Determination of the geocentric radii of density interfaces for each cell was done differently for both types of simulations our software is capable of. Where a single density interface is used, depths to the interface are read from an input file, e.g., a bathymetric model. The geocentric radius of the interface at any integration point is determined by $r_b(\Omega') = r_t(\Omega') - D_b(\Omega')$, where $D_b(\Omega')$ is the lake depth at the integration point, derived by bilinear interpolation of depths from the input file. The values of the densities above and below the interface are given in an option file, and these values are assigned to different segments according to the conditions from Eq. [8] or [9]. Where a geometrical figure is used to delineate a region of anomalous density, the determination of densities and density interfaces is more complicated.

The last but not least problem with numerical implementation is the behavior of the Newton kernel and its integrals and derivatives when the integration point is near to the computation point. We are dealing here with four different kernels: (a) the Newton kernel, used in Eq. [19]; (b) its radial derivative, used in Eq. [14]; (c) the integral of the Newton kernel with respect to the radius of the integration point, used in Eq. [26]; and (d) the integral of the radial derivative of the Newton kernel with respect to radius of the integration point, used in Eq. [24]. All these kernels have a point of singularity where $\psi = 0$ and $r = r'$. For our application this condition is easily resolved for the kernel in (b), since the computation point and integration point are always on the topographical surface and geoid respectively, so that this condition is only met when the height of the computation point is zero. In such situations, there can be no anomalous density at that point anyway (there is no topography) and so the value of the kernel at the point of singularity is exactly zero. For kernel (a) the singularity will always occur. Since r is always equal to r' over the region of integration, the singularity occurs

where $\psi = 0$, a point which must be included in any integration since it represents the value at the center of the spherical integration cap. For (c), the singularity will only occur when $\psi = 0$ and the top of the anomalous density body coincides with the topographical surface, since this is the only situation where r may equal r'. This singularity is easily remove in the case where anomalous density is considered relative to laterally varying surface density, since in that case the density anomaly whenever the body representing the density structure intersects the topographical surface its density is the surface density, and the anomalous density of the body itself is zero. Likewise, (d) can only be singular where $\psi = 0$ and the density body intersects the geoid.

These singularities are easily removed in terrain and 2-D anomalous density effect calculations. When used to calculate terrain effects, for example, it is clear that the terrain has the same height as does the Bouguer shell at the computation point (i.e. the central cell has zero contribution to the terrain effect), and so regardless of the singularity of the Newton kernel, the central cell contains no terrain and so the contribution of the central cell to the integration is zero (Martinec 1998). When dealing with laterally varying anomalous density, the contribution of a Bouguer shell of density equal to the anomalous density in the central cell can be added to the Newton integral to account for the contribution of the singularity point and take the integral without that differential neighbourhood of that point. Thus, at the central point the anomalous density relative to this shell is zero and, again, the singularity is removed (Martinec 1998).

While a similar approach could be applied for 3-D density effects, for this work we have simply arranged our integration points so that they do not correspond exactly with the computation point, so that the singularity does not occur. We recognize that this is not a

rigorous way of dealing with the immediate neighbourhood of the singularity, but for a first effort we consider our approach sufficient.

Numerical Stokes integration is required to evaluate Eqs. [15] and [22]. The integration is performed over a spherical cap of 4° radius, with cell size of 3', following the general procedure given in Heiskanen and Moritz (1967). The singularity of the Stokes kernel in the central cell is removed as suggested by Vaníček and Krakiwsky (1986).

Criteria for verification of results

For the purposes of this investigation, we will be testing our results for effects on gravity and gravity potential only. Our Stokes's integration contains no novel adaptations, while our Newton integration does, and is thus the focus of verifications.

We propose three methods of validating the results of our computations: (a) by examination the sequence of our results as the cell size used in numerical integration decreases, (b) by comparison with entirely analytical results for specific cases where such results can be found, and (c) by comparison with other similar efforts. Here we will be applying only (a) and (b), since while previous efforts similar to some of our simulations exist, we know of no other efforts which use directly a 3-D model of topographical density. The work of Martinec et al. (1995) on lake water effects, for example, does not use a 3-D model directly but instead uses a 3-D model based on bathymetry to create a 2-D laterally varying density model by averaging densities along the plumbline in each topographical column. The resulting 2-D model is then used in later calculations.

The testing in method (a) is done by first increasing the size of the innermost integration zone to approximately 3° in radius – normally the size of the middle zone. This is

much larger than it really needs be. Then the radii of other integration zones are also made equal to 3°, so that they are skipped in the numerical evaluation. Thus, all cells used in integration will have the same size, and the whole 3° spherical cap is covered. Next, the resolution of the innermost zone is varied from coarse to fine. As the resolution increases, we expect to see the results converge toward some particular value. If they do, then the results are at least consistent with each other.

Testing by method (b) provides a comparison with exact results in specific cases. The test we apply here is a comparison with an exact result for the DTE on gravity and PITE on gravity potential at a computation point on the axis of a spherical disc. The spherical disc is defined by the intersection of a cone and a spherical shell with its center at the apex of the cone. We examine the effect of a disc of a given size, oriented with its axis vertical, but with its mass center at various heights above the geoid.

To calculate exactly the PITE of the disc, we integrate Eqs. [18] and [19] setting $r = R$, over the region of a disc with a given density. We integrate in a geocentric spherical coordinate system, but to simplify the integration the primary axis is made coincident with the axis of the disc, so that when the dummy point of integration is at the computation point, $\psi = 0$. This provides for the effect of real topography on gravity potential at the geoid:

$$[27] \quad V^t_{\delta\rho}(\Omega = \Omega_c) = \pi G \delta\rho_D \left[\frac{2}{3} \frac{L^3_{g,u} - L^3_{g,l} - r^3_u + r^3_l}{R} + r^2_u - r^2_l + \cos(\psi_D) \left(L_{g,u} \left[r_u - R\cos(\psi_D) \right] - \right. \right.$$

$$\left. \left. - L_{g,l} \left[r_l - R\cos(\psi_D) \right] + R^2 \sin^2(\psi_D) \ln \left| \frac{r_u - R\cos(\psi_D) + L_{g,u}}{r_l - R\cos(\psi_D) + L_{g,l}} \right| \right) \right],$$

where r_l is the geocentric radius of the lower boundary of the disc, r_u is the geocentric radius of the upper boundary, ψ_D is the solid angle from the center of the disc to the edge, $\delta\rho_D$ is the anomalous density of the disc, and Ω_c is the spherical coordinates of the center of the disc. For conciseness, we have written straight-line distances using the convention $L_{p,q} = L(r_p, r_q, \psi_D)$. Where the term r_g is required to evaluate a distance, it is set to $r_g = R$.

For the effect of condensed topography on gravity potential at the geoid:

$$[28] \qquad V^c_{\delta\rho}(\Omega = \Omega_c) = 2\pi G \delta\sigma_D R \sqrt{2(1-\cos\psi_D)}\,,$$

where $\delta\sigma_D$ is the condensation density resulting from the anomalous density of the disc. By taking the derivatives of Eq. [27], we can also find the effect of real topography on gravity at the topographical surface:

$$[29] \qquad A^t_{\delta\rho}(\Omega = \Omega_c) = 2\pi G \delta\rho_D \left| L_{t,u}\left(\sin^2(\psi_D) - \frac{r_u}{r_t}\cos(\psi_D)\right) - L_{t,l}\left(\sin^2(\psi_D) - \frac{r_l}{r_t}\cos(\psi_D)\right) - \right.$$
$$\left. - \frac{L^3_{t,u} - L^3_{t,l} + r^3_u - r^3_l}{3r^2_t} + r_t\cos(\psi_D)\sin^2(\psi_D)\ln\left|\frac{L_{t,u} + r_u - r_t\cos(\psi_D)}{L_{t,l} + r_l - r_t\cos(\psi_D)}\right|\right|,$$

where $r_t = r_t(\Omega_c)$, and by taking the derivative of Eq. [26] we find the effect of condensed topography on gravity at the topographical surface:

$$[30] \qquad A^c_{\delta\rho}(\Omega = \Omega_c) = 2\pi G \delta\sigma_D \frac{r^2_g}{r^2_t}\left(\frac{r_t\cos\psi_D - r_g}{L_{g,t}} - 1\right).$$

We find from these results the DTE and PITE for Ω_c using Eqs. [12] and [17].

We evaluate the differences between results from these analytical formulas and from numerical determinations for the particular case of Ω_c to find an absolute determination of the error of our numerical approach in these particular cases, which we will take as an indicator of how well our approach might behave in other situations. Since this will only provide absolute errors for one set of situations, the resulting error estimates are not applicable for other simulations as anything more than an indicator of what we might expect the errors in those cases to be.

Results and discussion

Results demonstrating the capability of simulation software

We present here two sets of results. First as an example of a simulation of the effect of a simple density distribution, we present the effect on geoidal height of a disc representing a realistic density contrast, in topography of uniform height. From these results, we are able to observe some characteristics of the behavior of anomalous density effects. We finally provide an example of the 3-D anomalous density effect of a lake, again in smooth topography, as an example the effect of a density distribution given by a single density interface.

For the first simulation, we consider a density distribution given by a disc embedded in topography uniformly 2000 m thick. The disc itself is 40 km in diameter, and 500 m thick. We have assigned it a density of 660 kg/m^3, a typical anomalous density for, e.g., a disc of basalt

embedded in sandstone (e.g., Parasnis 1997). If the center of the disc is 500 m deep, it produces the DTE and PITE shown in Fig. 2. All figures show results over a 1° by 1° area.

Notice that with the DTE, the minimum of about -4 mGal is not at the center of the disc, but in a ring around the center. This is because the DTE is the difference between a contribution of real topography to surface gravity, and a slightly smoother contribution of condensed topography to surface gravity. The difference is constant near the projected center of the disc, but within the disc, moving away from its center, the contribution of real topography decreases more slowly than that of condensed topography, so that the difference between the two grows. However, around the edge of the disc the contribution of real topography diminishes rapidly, while the contribution of condensed topography diminishes more slowly. Thus the difference between the two grows smaller, and eventually changes sign, resulting in the ring of positive values surrounding the disc. The maximum result of 1.8 mGal occurs in this ring.

The same trend is not visible for the PITE, which has a minimum of about -19000 m*mGal at the disc center. Unlike the DTE, the PITE always decreases with distance from the disc center, since in the contribution of real topography decreases more rapidly than the contribution of condensed topography but is never less in magnitude than the contribution of condensed topography. For the same reason, the difference between the two contributions converges to zero, which is then the maximum value of the PITE.

Next we examine the effects resulting from this disc if it is rotated by certain angles around its west-east axis. In this case, we will present results from discs rotated by 0.5°, 1° and 5°. Here, we give the DTE and PITE on geoidal height. Also, the center of the disc is now situated at a depth of 1000 m. The SITE in these and all of our simulations so far is negligible. We further show the net effect on geoidal height resulting from both DTE and PITE. Results

for the DTE, PITE and total effect are given in Fig. 3. All figures show results over a 1° by 1° area.

First, notice that when the disc is nearly horizontal, the maximum value of the DTE on height is over the center of the disc. This is in contrast to the case with the DTE on gravity, and is a result of the smoothing effect of Stokes' integration used to determine the DTE on height. Also, the DTE and PITE tend to be larger where mass anomalies are distributed closer to the topographical surface. This is because both the DTE and PITE represent a difference between contributions of mass on the geoid and at the topographical surface, and these contributions are most different when the mass in real topography is distributed farther from the geoid. For this reason, the maximum values correspond to the part of the disc tilted toward the surface, and the minimum to the part tilted toward the geoid. In terms of magnitude, in the case where magnitudes are largest – where the disc is rotated to 5º from the horizontal – the DTE ranges from -0.2 cm to 1.0 cm, while the PITE ranges from 0 cm to 1.2 cm. However, due to the rotation of the discs these do not cancel each other where the positive effects are greatest. Thus the total effect ranges from -0.2 cm to 2.2 cm, which indicates that such a density body would have a significant effect on precise geoid determinations. These values are smaller in magnitude for other simulations. For comparison, Huang et al. (2001), using a 2-D density model in the Canadian Rocky Mountains, calculate anomalous density effects on the DTE ranging from -5.1 cm to 2.6 cm, the PITE ranging from -2.5 cm to 1.7 cm, and a total effect ranging from -7.0 cm to 2.8 cm. He finds that these effects are less than 10% of the effects calculated using a heterogeneous model of topographical density.

For our second simulation, we examine the 3-D anomalous density effects generated by Lake Superior. We will make some simple assumptions in this simulation. First, we consider all topography to have a thickness (height) of 183 m, about the average height of the

surface of Lake Superior. We also assume that the density of all topography in the area is 2670 kg/m^3, a common value for the average crustal density. The depths of the lake bed are given by a bathymetric data set prepared by Schwab and Seller (1996).

We are considering here the anomalous density relative to a laterally varying distribution, with densities equal to the density at the topographical surface. This is coherent with laterally varying density distributions based on densities from geology maps. Thus the laterally varying anomalous density is situated between the bed of the lake and the geoid, (where the lake bed is above the geoid). The results of the simulation are given in Fig. 4. We present results for the DTE and PITE on geoidal height. The SITE proved negligible. We also present the total effect of the DTE and the PITE. The results are distributed from latitudes of 46° to 50° north, and from longitudes of 264° to 274° east.

We notice especially here that the DTE on height is smoother than the PITE on height, due to smoothing of the DTE in Stokes integration. We also notice that, though there are some peaks in the PITE, the PITE is generally about an order of magnitude smaller than the DTE, and so the effects of the DTE are still dominant in the total effect. The DTE ranges from -8 mm to 9 mm, while the PITE is always positive and has a maximum magnitude of only 0.9 mm. Due to the small size of the PITE, the net effect is almost identical to the DTE.

Verification of results

Here we will apply the first of our suggested tests of our results. Since all vertical integration is analytical, only the horizontal integration in Eqs. [13], [14], [18] and [19] is performed numerically. Thus, as the horizontal integration step is decreased, the results should approach an exact result. If the results do not converge, there is some problem with our

approach. Note that while in this particular case the analytical results provide a more accurate estimation, the analytical result cannot yet be extended to any figure in spherical coordinates.

To visualize this test, we calculate the DTE on gravity and PITE on gravity potential for the projection of the center of a disc on the topographical surface and geoid respectively, as the depth of the disc is varied. We model a disc similar to the one used above, but only 200 m thick. The height of the center of the disc is varied from a height of 100 m to 1900 m. Note that at 1900 m, the top of the disc would actually be coincident with the surface of topography, a situation that cannot not possibly occur when considering anomalous density relative to a laterally varying distributions based on surface geology. Here we allow this situation to occur, so we can more fully examine the behavior of our results. Plots of the DTE and the PITE against the height of the disc center, for various horizontal integration step sizes, are given in Fig. 5.

We see that as the integration step is decreased, the results in both cases do converge. In the case of the DTE, the 3" and 1" lines are almost coincident except for a disc lying just under the surface. At that point, the DTE shows a slight increase for both. The same increase is much more noticeably for larger integration steps, and so is also apparently an artifact of the numerical integration. In the case of the PITE, the results converge very nicely to almost coincident lines. This indicates that our results are at least consistent with each other – at a given height, they converge to a single value. However, we must verify that they are approaching the correct result.

As an exact standard by which we may test our results, we apply Eqs. [27] to [30] to determine exactly the DTE on gravity and the PITE on gravity potential generated by the disc discussed in section 3.2. A comparison of the best 1" numerical integration results with the fully analytical result available for the particular case of a disc are shown in Fig. 6.

We see that the DTE from both results are nearly linear, but that the numerical result decreases more quickly than the analytical result. Thus the errors in the DTE grow as the depth to the density anomaly decreases. Although the sharp increase in the numerical result here makes it nearly coincident with the analytical result for a disc just below the topographical surface, we know from our previous comparison that this increase is an artifact of the numerical integration and so the coincidence of the two results at that point is only a fortunate canceling of errors, which will not usually occur.

For analysis of these results we will mainly discuss the percent differences between analytical and numerical results. This is expedient because it represents differences between the results in a way easily extrapolated to a crude estimate of errors for results in general, or of errors in effects on geoidal height. For example, if we know the difference between the numerical and analytical result in this particular case, where an analytical result is available for comparison, reaches a maximum of 20%, then we might guess that, e.g., our lake simulation result above has an error of 20% of the maximum effect of 9 mm, or about 2 mm. Of course this is a crude way of estimating errors, since results of other simulations may behave very differently from those for a disc. However, it is currently our only indication of absolute error in the results.

Considering only the situations where the disc does not touch the topographical surface, for a 1" integration step, the maximum percentage error in the DTE is 19%. In other simulations we have been able to achieve errors as large as 24%, but we are not especially concerned about these since the error is proportionally larger for thinner discs. For example, if we perform a simulation like that shown in Fig. 6 (a), but with a 400 m thick disc, we find the maximum percent error in the simulation is only 16%, while the maximum magnitude of results is 0.9 mGal. We find the greatest percent error, 23.5%, for a disc 200 m thick and 30

km wide, also in 2000 m thick topography. Thus, the formations with greatest influence on the DTE are also those whose effects, determined numerically, have the smallest relative error. This is also the width of disc that results in the smallest magnitude of DTE.

In the case of the PITE, both results are again nearly linear, but the numerical result here decreases more slowly than the analytical result with height of the disc center. Thus again the error in the PITE grows as depth to the disc decreases.

The percent error in the PITE is consistently much smaller than that in the DTE, reaching a maximum in this simulation of 4% for a disc near to the geoid. Note that the percent error in the PITE is smallest for narrower discs, and when the bottom of the disc is near to the geoid. Unlike the DTE, the PITE is greatest for thicker discs. The largest percent error we have found for the PITE is for a disc 5 km wide, and 1900 m thick, with its bottom at the geoid, in 2000 m thick topography, which yields an error of 7.6%.

We summarize in Table 2 below the worst errors we have been able to find in our results by comparison with an analytical result for a disc. For all of these situations, the simulations take place in 2000 m thick topography.

These results suggest maxima for our DTE and PITE results for the disc simulation, and suggest also some general principles for the sort of distributions where our numerical results might have lower accuracy. Considering that the maximum error for the DTE is just over 20 %, and that this decreases for larger values of DTE, we consider this sufficient validation of our approach for initial estimates of the order of magnitude of 3-D anomalous density effects.

Conclusions

Previous attempts to account for topographical density effects on geoidal height have modeled topographical density using a 2-D, laterally varying model. Since in reality topographical density also varies vertically, the 2-D model cannot account for all topographical density effects on geoidal height. We attempt to remedy this problem by modeling topographical density instead using surfaces representing topographical density interfaces. We calculate the DTE on gravity and PITE on gravity potential for any distribution by using Newton integration over a topographical density distribution defined by one or more interfaces, within a spherical cap. In the Newton integration, we use the analytical radially integrated Newton kernel and it's radial derivative to determine effects of density between interfaces, where it is piecewise constant. We then apply Stokes' integration to determine the DTE, PITE and SITE on geoidal height.

In this paper, we present results for the effects of a horizontal disc, for a disc rotated by various degrees along its longitudinal axis, and for the vertical density anomalies of Lake Superior. In all cases, we assume smooth topography and reasonable density contrasts, and consider anomalous density relative to a laterally varying density distribution. Total density effects of the disc on geoidal height reach 2.2 cm in magnitude when it is rotated by 5º, while those for the lake reach 0.9 cm in magnitude. We observe that the DTE and PITE both have their greatest magnitude for masses near to the topographical surface, and add rather than canceling each other each other for any of our disc simulations. In the case of the lake the effects are generally opposite, but do not significantly cancel each other out since the PITE is considerably smaller than the DTE.

We also attempt to validate our results by examination of the behavior of the DTE on gravity and PITE on gravity potential for the point at the center of a disc, at various depths in

topography. We find that as we decrease the horizontal integration step, the results in both of these cases converge, but do not converge exactly to a purely analytical result for the effect of the disc at these points. In our simulations, we find that the numerical DTE result is greater in magnitude than the analytical result, with a maximum error of 23.5 %. However, the greatest percent errors for this effect occur where the magnitudes of the effect are smallest, and in the worst case we have found the error is only 0.16 mGal in magnitude. Greater DTE errors occur where mass is concentrated near to the topographical surface, but where the mass is small. The numerical PITE result is consistently of lower magnitude than the analytical result, with maximum percent error of 7.6 %. In the case of the PITE, the greatest errors occur for discs near to the geoid, but when mass is great and the discs are small. Thus, for distributions having large effects, we expect the error in our calculation of those effects will be considerably smaller than the magnitudes suggested here.

Future efforts will include more thorough treatment of the singularity of the Newton kernel as applied in a 3-D density modeling context, as well as investigation and mitigation of the errors we have detected in our numerical results. However, with our efforts so far, we can suggest that 3-D anomalous topographical density may have centimeter-level contributions to the geoidal height in some situations. Whether those situations are common is yet to be seen.

Acknowledgements

We are grateful for the reviewers of this manuscript, and the Associate Editor of CJES, whose comments have made the final product much more approachable and complete. This research was funded mainly by a scholarship from the National Sciences and Engineering

Research Council (NSERC) for funding most of this research.

References

Bassin, C., Laske, G. and Masters, G. 2000. The Current Limits of Resolution for Surface Wave Tomography in North America. *EOS*. **81**: F897.

Heck, B. and Seitz, K. 2007. A comparison of the tessaroid, prism and point-mass approaches for mass reductions in gravity field modelling. *Journal of Geodesy*. **81**: 121-136.

Heiskanen, W., and Moritz, H. 1967. Physical Geodesy. W.H. Freeman and Co., San Francisco.

Helmert, F. 1884. Die mathematischen und physikalischen Theorieen der höheren Geodäsie, vol. 2, Leipzig, B.G. Teubner.

Huang, J., Vaníček, P., Pagiatakis, S., and Brink, S. 2001. Effect of topographical density variation on geoid in the Canadian Rocky Mountains. Journal of Geodesy, **74**: 805-815.

Kuhn, M. 2003. Geoid determination with density hypotheses from isostatic models and geological information. Journal of Geodesy, **77**: 50-65.

Martinec, Z. 1993. Effect of lateral density variations of topographical masses in improving geoid model accuracy over Canada. Contract report for Geodetic Survey of Canada, Ottawa.

Martinec, Z., and Vaníček, S. 1994a. The indirect effect of topography in the Stokes-Helmert technique for a spherical approximation of the geoid. Manuscripta Geodaetica **19**: 213-219.

Martinec, Z., and Vaníček, P. 1994b. Direct topographical effect of Helmert's condensation for a spherical approximation of the geoid. Manuscripta Geodaetica, **19**: 257-268.

Martinec, Z., Vaníček, P., Mainville, A., and Véronneau, M. 1995. The effect of lake water on geoidal heights. Manuscripta Geodaetica, **20**: 193-203.

Martinec, Z. 1998. Boundary Value Problems for Gravimetric Determination of a Precise Geoid (Lecture Notes in Earth Sciences). Springer-Verlag, New York.

Mooney, W., Laske, G. and Masters, T. 1998. CRUST 5.1: A global crustal model at 5º x 5º. *Journal of Geophysical Research*. **103**: 727-747.

Mooney, W. 2007. Crust and Lithospheric Structure – Global Crustal Structure. *In* Treatise on Geophysics: Volume I – Seismology and Structure of the Earth. *Edited by* G. Schubert. Elsevier Science, Amsterdam, pp. 361-417.

Moritz, H. 1984. Geodetic Reference System 1980. Bulletin Géodésique, **58**: 388-398.

Nagy D., Papp, G., and Benedek, J. 2000. The gravitational potential and its derivatives for the prism. Journal of Geodesy, **74**: 552-560.

Parasnis, D. 1997. Principles of Applied Geophysics. Chapman and Hall, New York.

Pasyanos, M., Walter W., Flanagan, M., Goldstein, P. and Battacharyya, J. 2004. Building and Testing an a priori geophysical model for Western Eurasia and North Africa. *PAGEOPH* **161**: 235-281.

Paul, M. 1974. The gravity effect of a homogeneous polyhedron for three-dimensional interpretation. Pure and Applied Geophysics. **112**: 553–561.

Pohanka, V. (1998) Optimum expression for computation of the gravity field of a polyhedral body with linearly increasing density. *Geophysical Prospecting*. **46**: 391–404.

Salah, M. and Zhao, D. 2003. 3-D seismic structure of Kii peninsula in southwest Japan: evidence for slab dehydration in the forearc. Tectonophysics. **364**: 191-213.

Schwab, D., and Sellers, D. 1996. Computerized Bathymetry and Shorelines of the Great Lakes. NOAA Data Report ERL GLERL-16, Great Lakes Environmental Research Laboratory, Ann Arbor, Michigan.

Sjöberg, L., and Nahavandchi, H. 1999. On the indirect effect in the Stokes-Helmert method of geoid determination. Journal of Geodesy, **73**: 87-93.

Smithson, S., Wenzel, F., Ganchin, Y. and Morozov, I. 2000. Seismic results at Kola and KTB deep scientific boreholes: velocities, reflections, fluids, and crustal composition. Tectonophysics. **329**: 301-317.

Soller, D., Ray R. and Brown, R. 1982. A new global crustal thickness model. Tectonics. **1**: 125-149.

Stokes, G. 1849. On the variation of gravity on the surface of the Earth. Transactions of the Cambridge Philosophical Society, **8**: 672-695.

Tiberi, C., Diament, M., Déverchère, J., Petit-Mariani, C., Mikhailov, V., Tikhotsky, S. and Achauer, U. 2003. Deep structure of the Baikal rift zone revealed by joint inversion of gravity and seismology. Journal of Geophysical Research. **108**: (doi:10.1029/2002JB001880).

Tsoulis, D. 2001. Terrain correction computations for a densely sampled DTM in the Bavarian Alps. Journal of Geodesy. **75**: 291–307.

Tziavos I., and Featherstone, W. 2000. First results of using digital density data in gravimetric geoid computation in Australia. *In* Gravity, geoid and geodynamics. *Edited by* Sideris, M.G. Springer, New York, pp 335–340.

Vaníček, P., and Krakiwsky, E. 1982. Geodesy: The Concepts. North-Holland, New York.

Vaníček, P., and Kleusberg, A. 1987. The Canadian geoid – Stokesian approach. Manuscripta geodetica, **12**: 86-98.

Vaníček, P., and Martinec, Z. 1994. The Stokes-Helmert scheme for the evaluation of a precise geoid. Manuscripta Geodaetica **19**: 119-128.

Vaníček, P., Huang, J., Novak, P., Pagiatakis, S., Veronneau, M., Martinec, Z. and Featherstone, W. 1999. Determination of the boundary values for the Stokes-Helmert problem. Journal of Geodesy, **73**: 180-192.

Zelt, C. and Smith, R. 1992. Seismic traveltime inversion for 2-D crustal velocity structure. Geophysical Journal International. **108**: 16-34.

Zelt, C. 1999. Modelling strategies and model assessment for wide-angle seismic traveltime data. Geophysical Journal International. **139**: 183-204 (22).

Figure Captions

Fig. 1: Spherical coordinate system for evaluation of Newton integrals.

Fig. 2: DTE on gravity and PITE on gravity potential resulting from a disc 500 m thick, 40 km in diameter, with anomalous density of 660 kg/m^3, with center 500 m deep, embedded in 2000 m thick topography.

Fig. 3: DTE, PITE and the total effect of anomalous density on geoidal height for discs 500 m thick, 40 km in diameter, with anomalous density of 660 kg/m^3, with centers 1000 m deep, embedded in 2000 m thick topography, and rotated to 0.5º, 1º and 5º from horizontal.

Fig. 4: Effects of 3-D anomalous density of Lake Superior on geoidal height.

Fig. 5: DTE and PITE against height to disc center for discs 200 m thick, 40 km in diameter, with anomalous density of 660 kg/m^3, embedded in 2000 m thick topography, with varying heights to disc center and with varying horizontal integration intervals.

Fig. 6: DTE and PITE against height to disc center for discs 200 m thick, 40 km in diameter, with anomalous density of 660 kg/m^3, embedded in 2000 m thick topography, with varying heights to disc center of varying, from both analytical integration and from numerical integration with 1" step.

Table 1: Integration zone sizes and resolutions

Zone	Radius (arcseconds)	Resolution (arcseconds)
Middle	7200	300
Inner	3600	30
Innermost	1080	3
Central	1.5	1

Table 2: Worst case errors to date for DTE and PITE, determined by comparison with an analytical result for a disc having density contrast of 660 kg/m^3 in 2000 m thick topography.

	DTE	PITE
analytical result	-0.67 mGal	-38239 m*mGal
numerical result	-0.82 mGal	-35317 m*mGal
difference	-0.16 mGal	2922 m*mGal
% error	23.5 %	7.6 %
disc width	30 km	5 km
disc thickness	200 m	1900 m
depth to disc center	200 m	1050 m

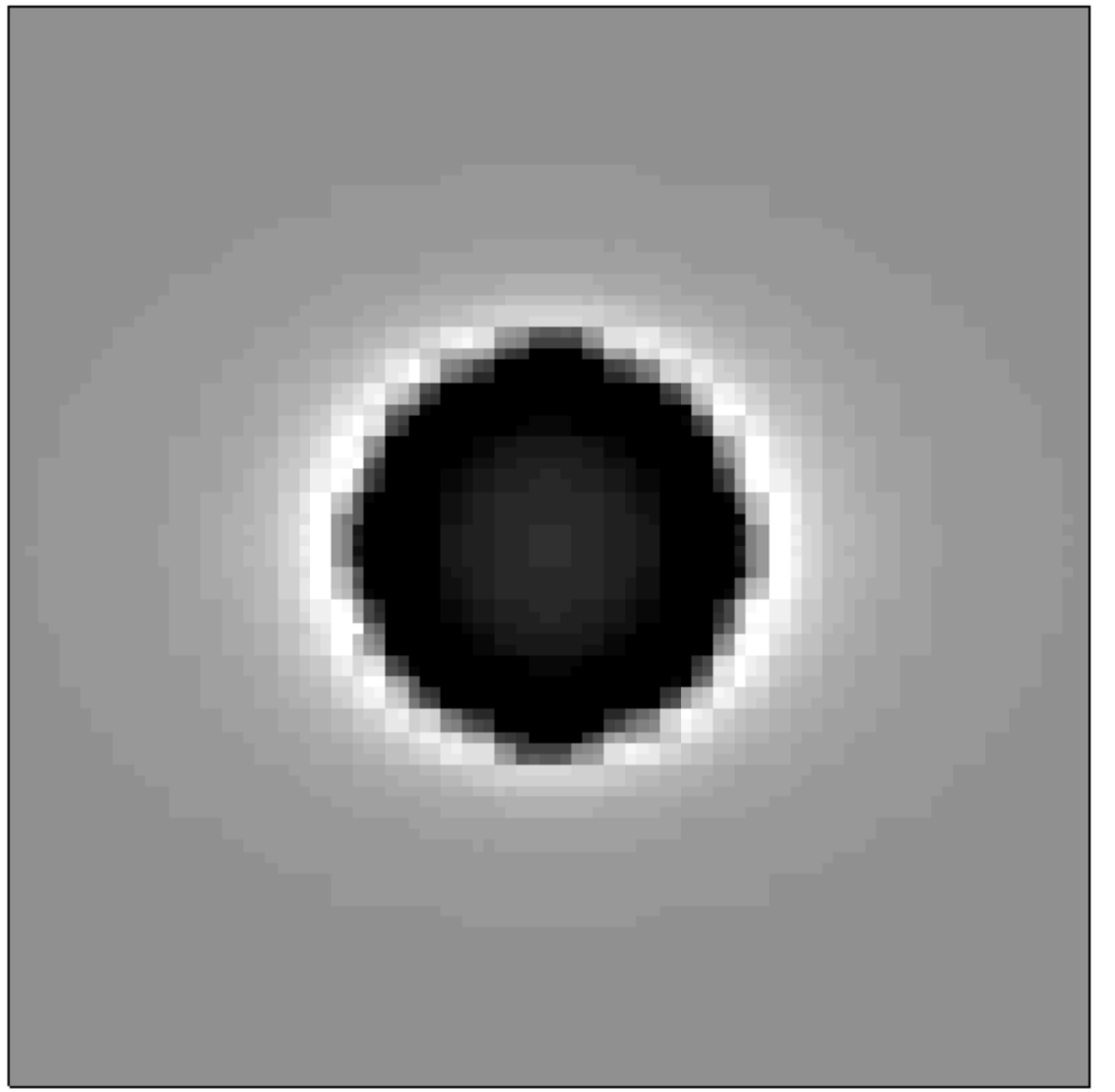

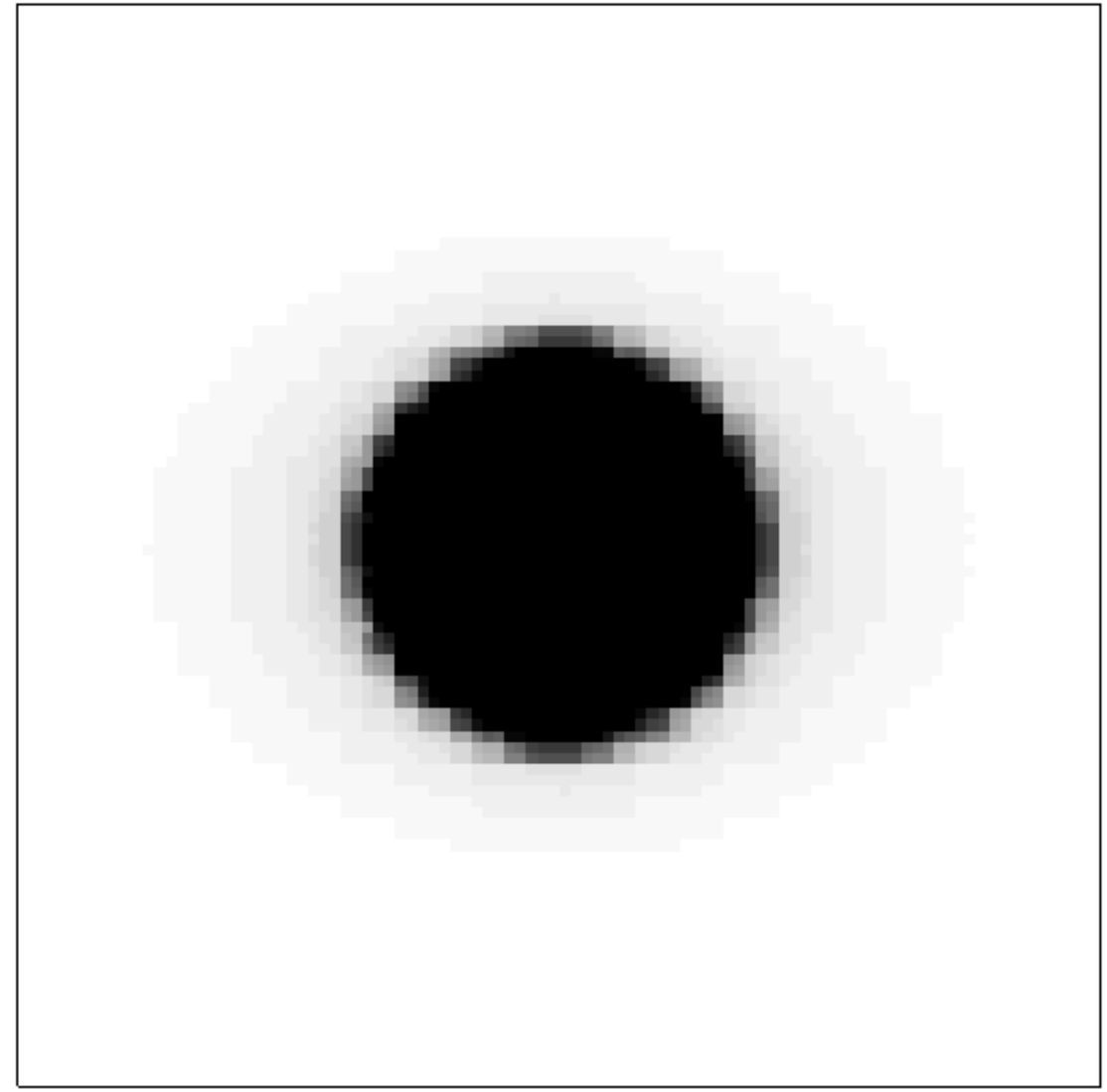

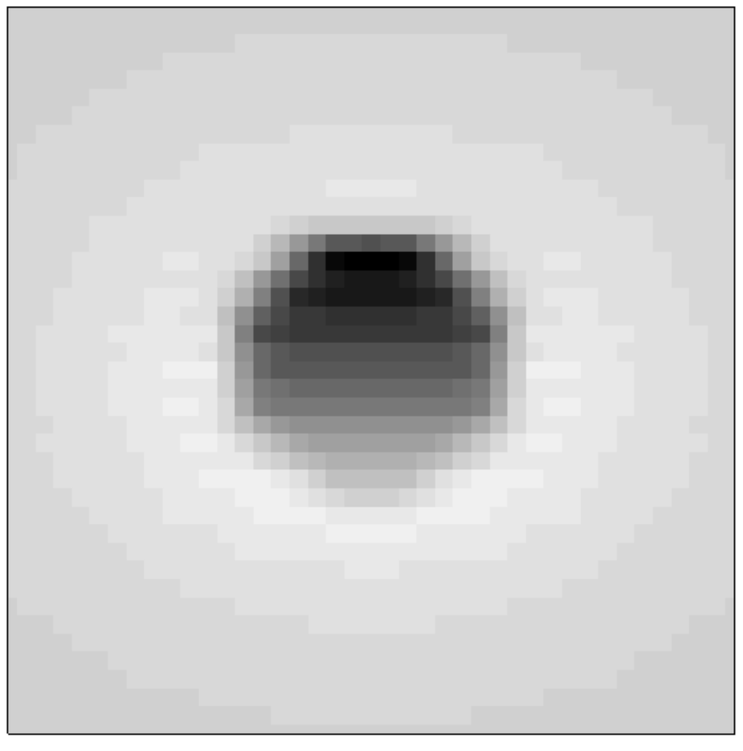

−0.010 −0.008 −0.006 −0.004 −0.002 0.000 0.002

direct topographical effect on geoid height (meters)

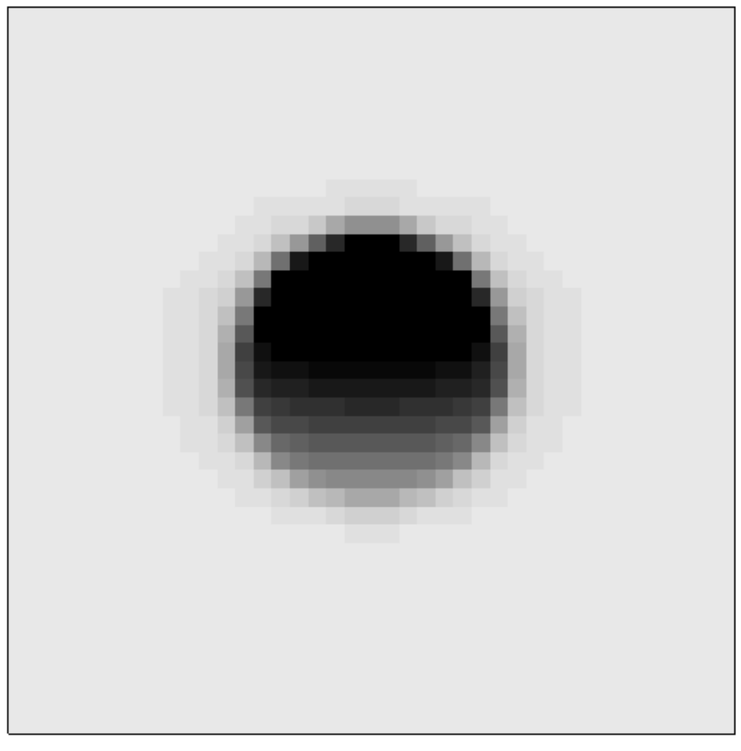

−0.012 −0.010 −0.008 −0.006 −0.004 −0.002 0.000

primary indirect topographical effect on geoid height (meters)

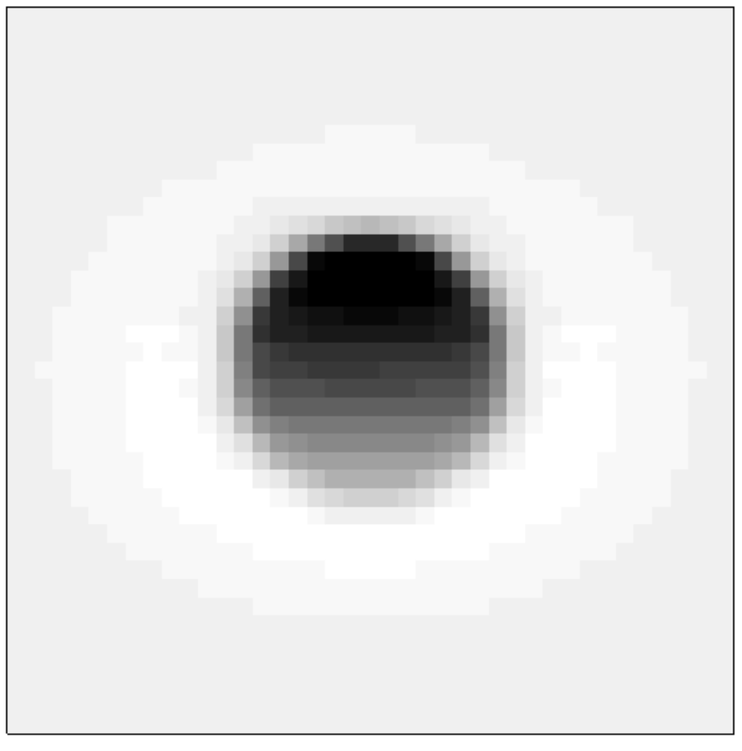

−0.025 −0.020 −0.015 −0.010 −0.005 0.000

total effect on geoid height (meters)

0.5°

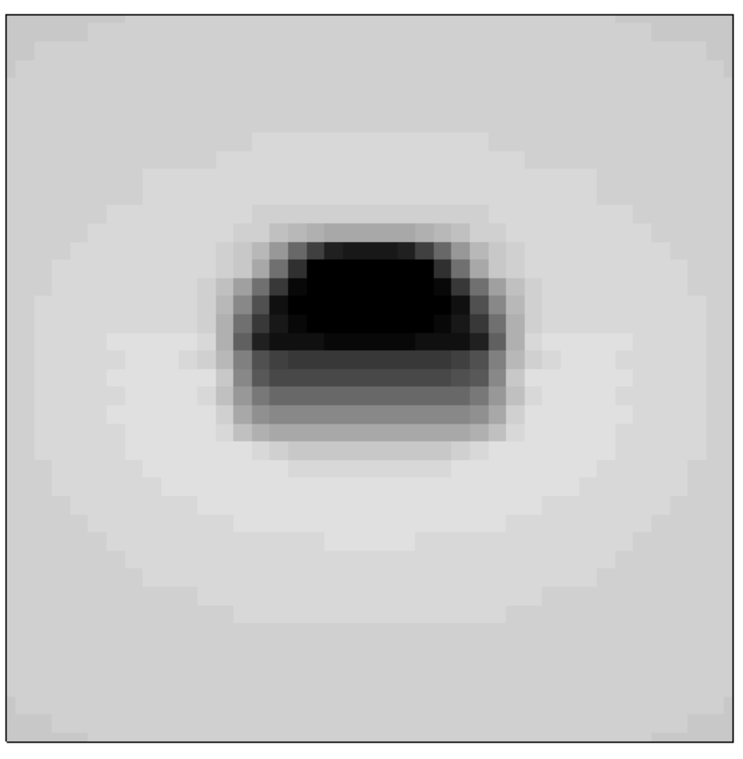

−0.010 −0.008 −0.006 −0.004 −0.002 0.000 0.002

direct topographical effect on geoid height (meters)

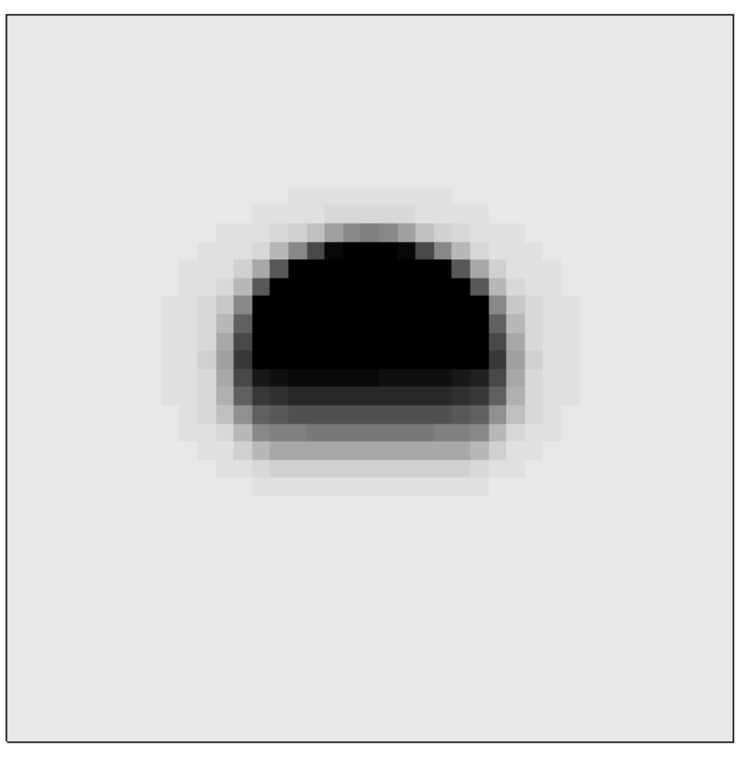

−0.012 −0.010 −0.008 −0.006 −0.004 −0.002 0.000

primary indirect topographical effect on geoid height (meters)

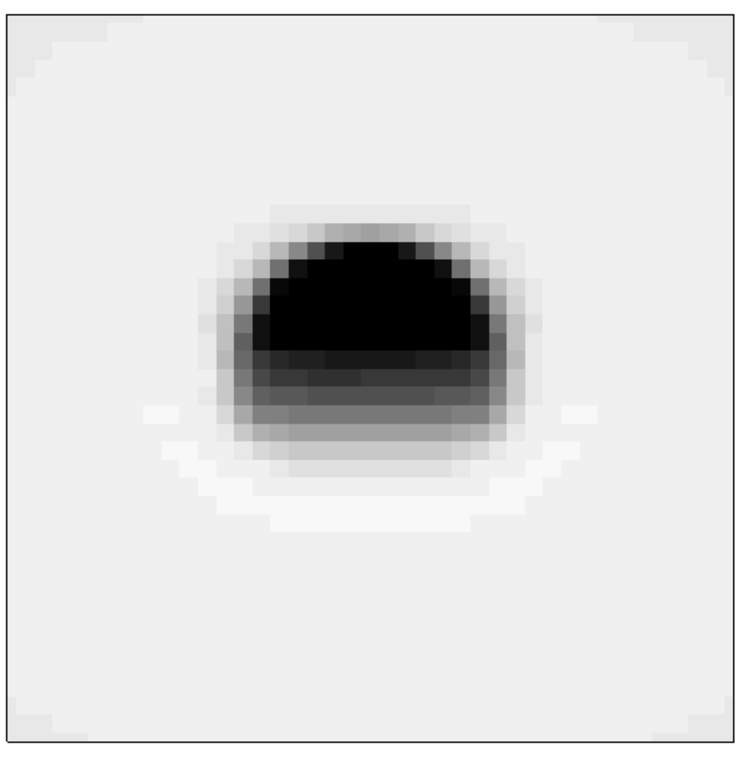

−0.025 −0.020 −0.015 −0.010 −0.005 0.000

total effect on geoid height (meters)

1.0°

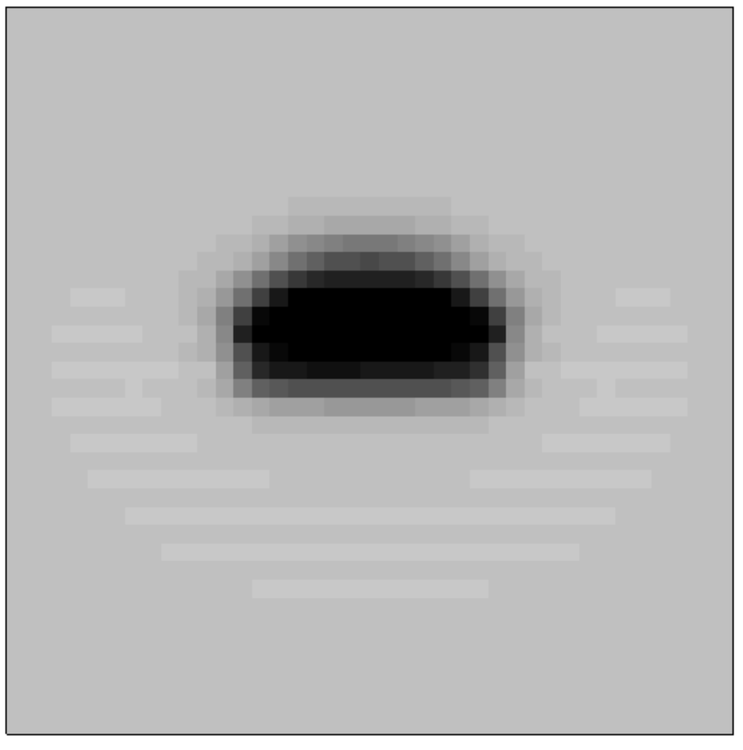

−0.010 −0.008 −0.006 −0.004 −0.002 0.000 0.002

direct topographical effect on geoid height (meters)

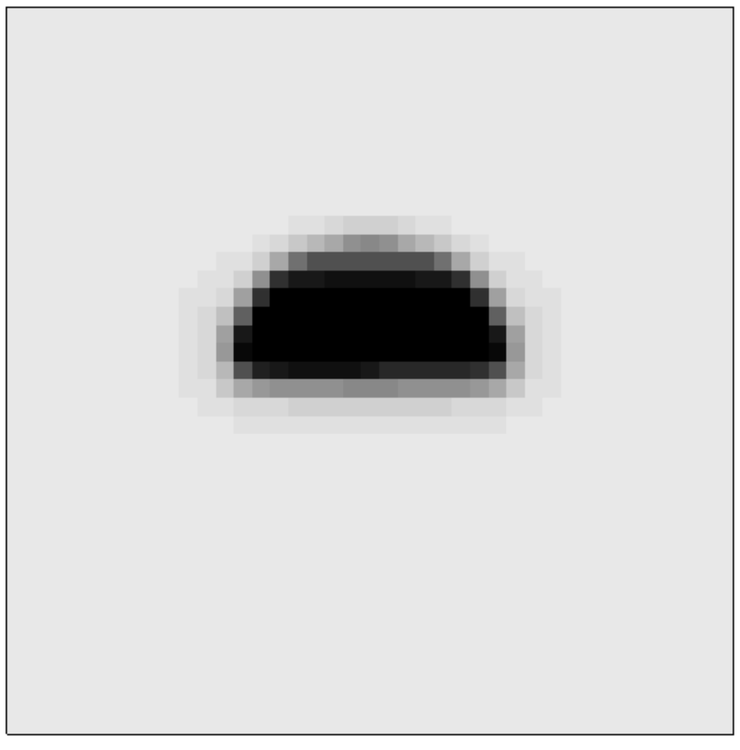

−0.012 −0.010 −0.008 −0.006 −0.004 −0.002 0.000

primary indirect topographical effect on geoid height (meters)

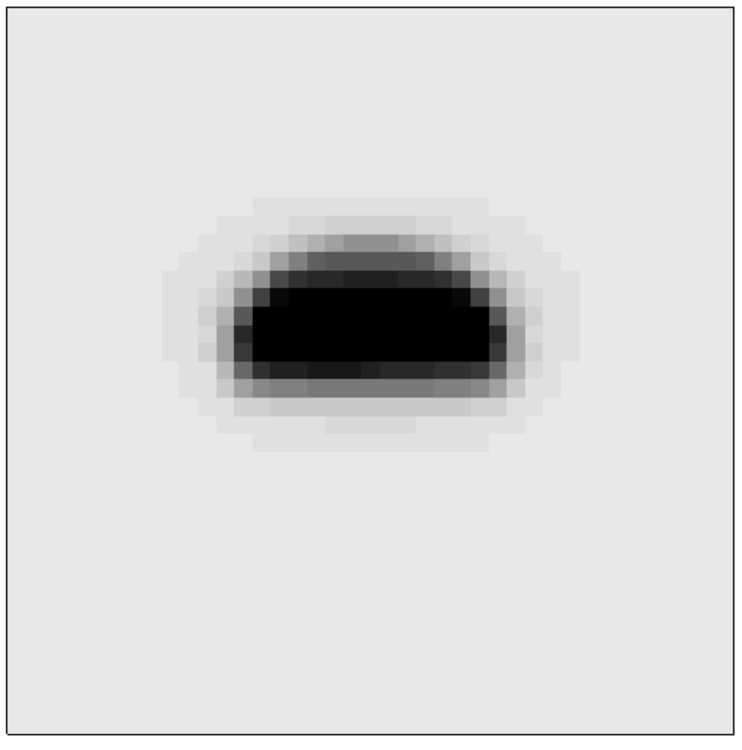

−0.025 −0.020 −0.015 −0.010 −0.005 0.000

total effect on geoid height (meters)

5.0°

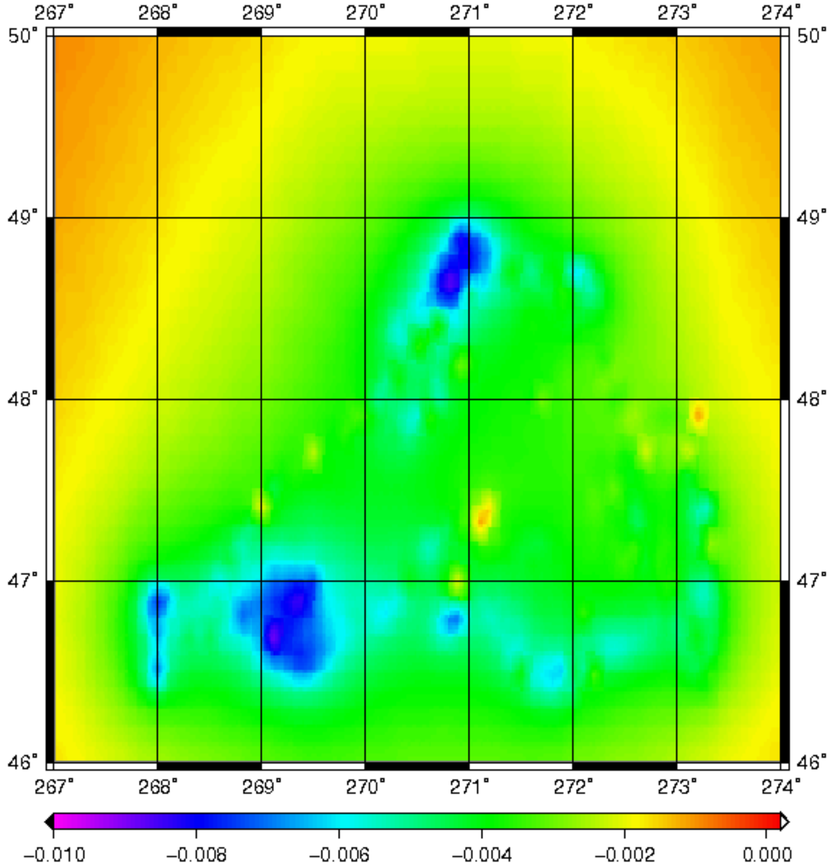

direct topographical effect on geoid height (meters)

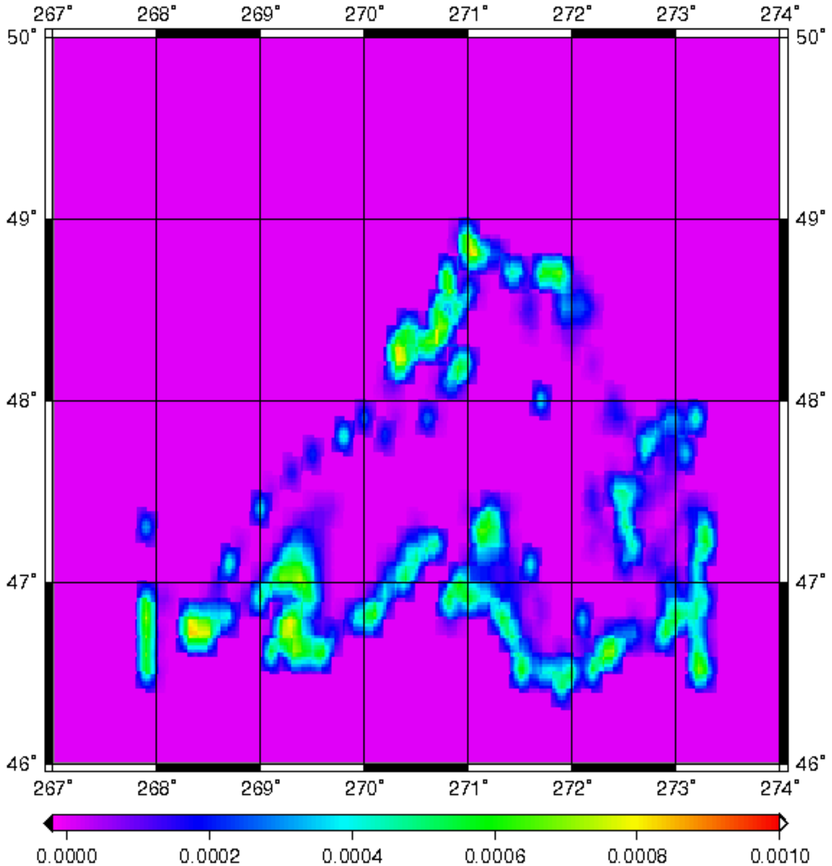

primary indirect topographical effect on geoid height (meters)

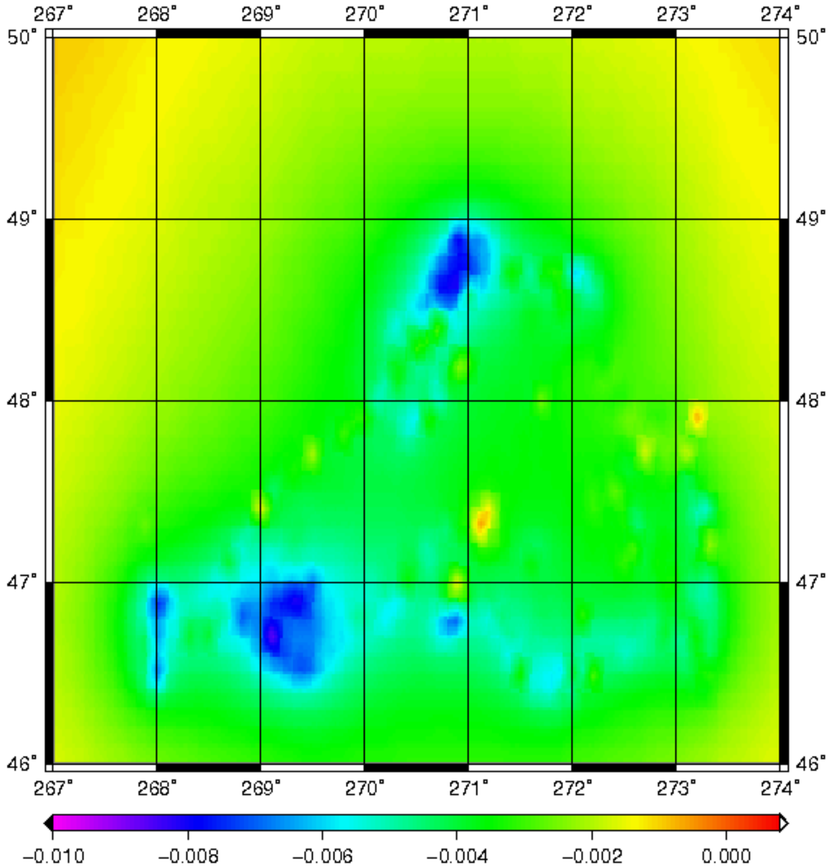

total effect on geoid height (meters)